Research in Astronomy and Astrophysics, 25:015005 (9pp), 2025 January

https://doi.org/10.1088/1674-4527/ad95d8
CSTR: 32081.14.RAA.ad95d8

A Method to Assess the Applicability and Accuracy of the Modified Gaussian Model (MGM) on the Rock Samples' Spectral Interpretation

Fang Gao[1,2,3,4], Bin Liu[1,2], Qin Zhou[1,2,4], and Chun-Lai Li[1,2]
[1] Key Laboratory of Lunar and Deep Space Exploration, Chinese Academy of Sciences, Beijing 100012, China; liub@nao.cas.cn
[2] National Astronomical Observatories, Chinese Academy of Sciences, Beijing 100012, China
[3] University of Chinese Academy of Sciences, Beijing 100049, China
Received 2024 June 01; revised 2024 November 02; accepted 2024 November 10; published 2025 January 2

Abstract

The Chang'e-4 mission obtained spectral data of multiple rock targets on the lunar surface. The Modified Gaussian Model (MGM) is usually applied to the spectral interpretation of powder samples, its applicability and accuracy on the rock targets remain to be further evaluated. The rock slice of lunar meteorite NWA 4734 is used to conduct comprehensive analysis of the petrography, mineralogy and laboratory spectroscopy, which will provide important ground truth for the MGM interpretation of lunar in situ spectra of rock samples. First, a scanning electron microscope (SEM), Energy Dispersive Spectrometer (EDS), and Electron Probe Micro-Analyzer (EPMA) analysis results indicate that: (1) almost all plagioclase in NWA 4734 have been converted to maskelynites, which indicate that the meteorite has undergone severe impact metamorphism; (2) the chemical composition of pyroxene and olivine is significantly heterogeneous, showing a distribution characteristic of magnesium-rich core and iron-rich rim, further indicating that NWA 4734 has undergone multiple crystallization and differentiation. Second, this article focuses on the rock slice of NWA 4734's greyscale image of the Back Scattering Electron (BSE), and obtains the proportion of High-Calcium Pyroxene (HCP) in the total pyroxenes of this sample by calculating the area percentage using the pixel counting method. The result shows that the proportion of HCP is $72\% \pm 5.4\%$, which can be used as a ground truth to evaluate the interpretation applicability and accuracy of MGM. A field spectrometer (ASD) is used to measure the visible and near-infrared reflectance spectra (450–2500 nm) of the rock slice from NWA 4734 in the same area as the BSE image obtained by SEM, and MGM is used to deconvolve the ASD spectra, and the average proportion of HCP is estimated to be $71\% \pm 10.1\%$. The results between the MGM and the pixel counting are comparable within the error range, which demonstrates the applicability of MGM on interpretation of the rock samples on the lunar surface.

Key words: astrochemistry – methods: data analysis – instrumentation: spectrographs

1. Introduction

The Chang'e 4 mission has completed spectral detection of multiple rock targets in the landing area, while the Chang'e 5 mission successfully returned 1731 grams of lunar samples, which also included many rock chip samples. So, laboratory studies on the rock samples' composition and spectral characteristics can support the interpretation of the in situ spectral data of lunar rock targets. However, the most rock chip samples collected by the Chang'e 5 mission have small particle sizes (<1 cm), which are difficult to meet the laboratory non-imaging visible and near-infrared spectral test requirements (the particle sizes of the samples generally need to be >1 cm).

Lunar meteorites are also important samples for our laboratory research. Currently, the returned lunar samples only cover a small portion of the near side of the Moon, while lunar meteorites, coming from different places on the lunar surface, are important complementary samples for our research. Northwest Africa (NWA) 4734 is a lunar basaltic meteorite that represents the composition of lunar maria basalt. Currently, many works on the lunar meteorite NWA 4734 have been done. Wang et al. (2012b) reported the petrography, mineralogy, geochemistry and Pb-Pb geochronology of the lunar meteorite NWA 4734 (Wang et al. 2012b), Elardo et al. (2014) conducted geochemical, petrological, mineralogical, and Sm-Nd, Rb-Sr, and Ar-Ar isotopic studies on NWA 4734 (Elardo et al. 2014); Chen et al. (2019) also studied NWA 4734 together with NWA 10597 (Chen et al. 2019). All above works demonstrated that NWA 4734 and the LaPaz Icefield (LAPs) low-Ti lunar basaltic meteorites have similar textures, modal abundances, mineral chemistry, and crystallization ages, which most likely originated from the same region of the Moon and both experienced intensive shock events (Fernandes et al. 2009; Jambon & Devidal 2009). These results indicate that NWA 4734 has undergone intense impact metamorphism (Wang et al. 2012a)

[4] Both authors contributed equally to this work.

and multistage crystal differentiation (Chen et al. 2019), with a radioactive isotope age of approximately 3 billion years (Elardo et al. 2014), making it a representative product of young, highly evolved volcanic activity on the lunar surface. However, there is little visible or near-infrared spectral analysis of this meteorite rock sample. Acquiring the visible and near-infrared spectra of NWA 4734, combined with the existing petrography and mineralogy results, can provide ground truth for the interpretation of in situ spectra of lunar rock targets.

The Modified Gaussian Model (MGM) is an important method for interpreting the visible and near-infrared spectra of minerals (Sunshine & Pieters 1993). This model assumes that the absorptions of materials are composed of a series of Gaussian curves, and the compositional variability of the primary absorption bands that constitute the diagnostic features of pyroxene and olivine can be quantified by examining the band centers and relative strengths (Sunshine et al. 1990; Sunshine & Pieters 1998; Isaacson & Pieters 2010; Crown & Pieters 1987), with a model error of about 5%–10% (Sunshine & Pieters 1993). The specific interest of this model is to directly account for electronic transition processes (Sunshine et al. 1990). Consequently, the MGM approach is in essence able to achieve a direct detection and quantification of minerals' composition (Clénet et al. 2011). Sunshine and Pieters first dealt with simple minerals or mixtures (i.e., either olivine and pyroxene alone or the pyroxene mixtures) using this model (Sunshine & Pieters 1993, 1998). Three Gaussian functions were used in the model to characterize systematic trends linked to M1 and M2 sites for olivine, and the results indicate that with the progressive increase of iron content, the absorption band centers gradually increase toward the direction of longer wavelengths, and the intensity of the 1.05 μm band gradually increases relative to the 1.2 μm feature. The width did not show any particular trend. Sunshine & Pieters (1993) also use MGM to deconvolve the mixture spectra of two pyroxene end-members, High-Calcium Pyroxenes (HCPs) and Low-Calcium Pyroxenes (LCPs), with fixed compositions, and the results showed that the relative abundance of the two pyroxenes can be directly correlated with the Gaussian intensity ratios, while the centers and widths of the absorption bands did not depend on the mineral proportions (Sunshine & Pieters 1993). MGM was applied to remote sensing near-infrared spectra to extract relative abundance of HCP and LCP for studying a planetary surface's mineralogy and geology (Mustard & Sunshine 1995; Mustard et al. 1997; Gendrin et al. 2006; Noble et al. 2006; Kanner et al. 2007). However, there are still some controversies in the application of MGM in laboratory and remote sensing data interpretation (Pieters et al. 1993; Cheek & Pieters 2014). For example, Kanner et al. (2007) analyzed the applicability of MGM in remote sensing data, and the results showed that MGM would behave well when the data have high signal-to-noise ratio, and the content of olivine in the target cannot exceed 15%. Moreover, MGM was mainly applied to the interpretation of powder samples, but rarely to explore complex mixtures of minerals and/or rock samples. The interpretation capability of MGM needs to be improved to realistically model a complicated lunar basaltic meteorite.

Figure 1. The rock slice of lunar basaltic meteorite NWA 4734.

This paper will first analyze the petrography and mineralogy of NWA 4734, with the aim to further constrain whether it experienced intense impact metamorphism and multistage crystal differentiation. Second, the petrographic results, mineralogical results and the high-resolution Back Scattering Electron (BSE) image of NWA 4734, obtained by a scanning electron microscope (SEM), will be used to accurately calculate the proportion of HCP and LCP using the image pixel counting method, and the proportion of HCP and LCP will be used as a ground truth to evaluate the applicability and accuracy of MGM for the rock samples.

2. Samples and Analytical Methods

2.1. Sample Description

The meteorite NWA 4734 used in this study is a rock slice with a length of ~5 cm, a width of 3 cm, a thickness of 0.8 cm, and a total mass of 21.2 g (Figure 1). The grain size of the minerals is coarse, and the composition is mainly composed of millimeter-sized phenocryst-like augite and maskelynite, with a small amount of ilmenite, pyrrhotite, baddeleyite, zirconolite, and tranquillityite (Wang et al. 2012b). Similar to shergottite, almost all the feldspar has been transformed into maskelynite, and the pyroxene particles have developed cleavage.

2.2. SEM and EDS Analysis of the Sample

The Zeiss field emission SEM SUPRA55 was used to obtain petrographic and mineralogical information, with a resolution of 0.8 nm @15 kV, an acceleration voltage of 15 kV, a working distance of 8.2 mm and a magnification of 50 times. In order to simultaneously obtain the minerals' content and spectral characteristics at the same location, instead of preparing into a polished section, the surface of the rock slice was ground and

polished, and then was directly placed under the SEM to obtain the petrographic information.

2.3. EPMA Analysis of the Sample

The JEOL JXA-8230 Electron Probe Micro-Analyzer (EPMA) is used to determine the major elements' content of feldspar, pyroxene, olivine and other silicate minerals. The EPMA is also equipped with an Energy Dispersive Spectrometer (EDS) to identify mineral types, to help select suitable areas to avoid the influence of cracks and mineral inclusions. The working voltage for EPMA is set as 15 kV, the electron beam current is 10 nA, and the diameter of the beam spot is 5 μm. The measurement times of the signals and backgrounds for each element are set to 20 s and 10 s, respectively. The natural minerals and synthetic glasses are selected as calibration standards, with oxide detection limits of 0.01–0.03 wt% for most elements. All the data have been corrected for the ZAF (atomic number, X-ray absorption, fluorescence) (Wang et al. 2012b).

2.4. Calculating the Proportion of HCP Using Image Pixel Counting Method

There is a definition difference of HCP between mineralogy and spectroscopy. In mineralogy, the HCP is defined as pyroxenes which have a value of Wo > 95, but in spectroscopy, the HCP is defined as pyroxenes with a value of Wo > 80, Wo = CaO(Wt%) /56/(CaO(Wt%)/56+MgO(Wt%)/40+FeO (Wt%)/72). In this study, we selected the definition of HCP with a value of Wo > 80. The image pixel counting method for estimating the proportion of HCP is as follows: (1) perform greyscale processing on the BSE image to assign each mineral type to a determined greyscale value in the range of 0–256, and different mineral compositions are determined by EDS in different greyscale regions. This method can eliminate the statistical errors caused by the uneven distribution of mineral components in the BSE image. (2) The regions with determined components (HCP or LCP) are processed using photoshop software, red and blue colors are used to distinguish between LCP and HCP, and the tolerance is set as 5%. The pixel counts of the red and blue regions are counted, and the ratio of the pixel counts between the red and blue regions, corresponding to the area of the HCP and LCP, is calculated. The tolerance is a main source of error, with an estimated error value of 5%.

2.5. Calculating the Proportion of HCP Using MGM

An ASD spectrometer (Field Fieldspec4) is used to obtain the visible and near-infrared spectra of NWA 4734. The spectral range of the ASD is 350–2600 nm, with the spectral resolutions being 3 nm@700 nm, 10 nm@1400 nm and 2100 nm. The spectral sampling intervals are 1.4 nm@350–1050 nm and 2 nm@1000 nm–2500 nm. The spectral measurement environment is a darkroom without incident stray light.

Figure 2. Full BSE image of the rock sample NWA 4734. The red circle shows the area measured by the ASD and it is also the area for the image pixel count of HCP and LCP.

The area of the red circle plotted in Figure 2 is measured by ASD, and the field of view is 3°; the height and position of the sample are adjusted so that the measurement is a circular area with a radius of 1.5 cm, which coincides with the areas of HCP and LCP counted in the BSE image.

The method for MGM interpretation is as follow: (1) a type of continuum needs to be selected and the parameters such as slope and intercept should be initially set. (2) select proper numbers of Gaussian curves with curve centers, widths and depths initially set. (3) decompose the actual spectrum into the continuum and numbers of Gaussian curves, adjust parameters, such as the number of Gaussian curves, curve centers, widths or depths, to make the superposition of the continuum and the Gaussian curves as close to the actual measured spectrum as possible until the error is acceptable. A relationship between the depth ratios of the Gaussian curves and the proportion of HCP in total pyroxenes was found by Sunshine & Pieters (1993). Based on this relationship, we could calculate the proportion of HCP in total pyroxenes.

3. Results and Discussion

3.1. Petrographic Characteristics

The BSE image of NWA 4734 is shown in Figure 3. We can see that the particle sizes of pyroxene in NWA 4734 are slightly larger than those of plagioclase, which is distributed in the shape of euhedral lath. The xenomorphic granular pyroxene fills in the triangular gaps are formed by the lath grains of plagioclase, forming a diabase texture. Most individual plagioclase particles are elongated, 5–10 μm in size, with a directional distribution trend (Figure 3(a)). Generally, the plagioclase particles have a distribution characteristic of small sizes in the middle and large sizes at the rim, and there are symplectites. The content and sizes of plagioclase are second only to pyroxene, and almost all plagioclase has been transformed into maskelynite after impact metamorphism. From the BSE image we could also see that the greyscale of

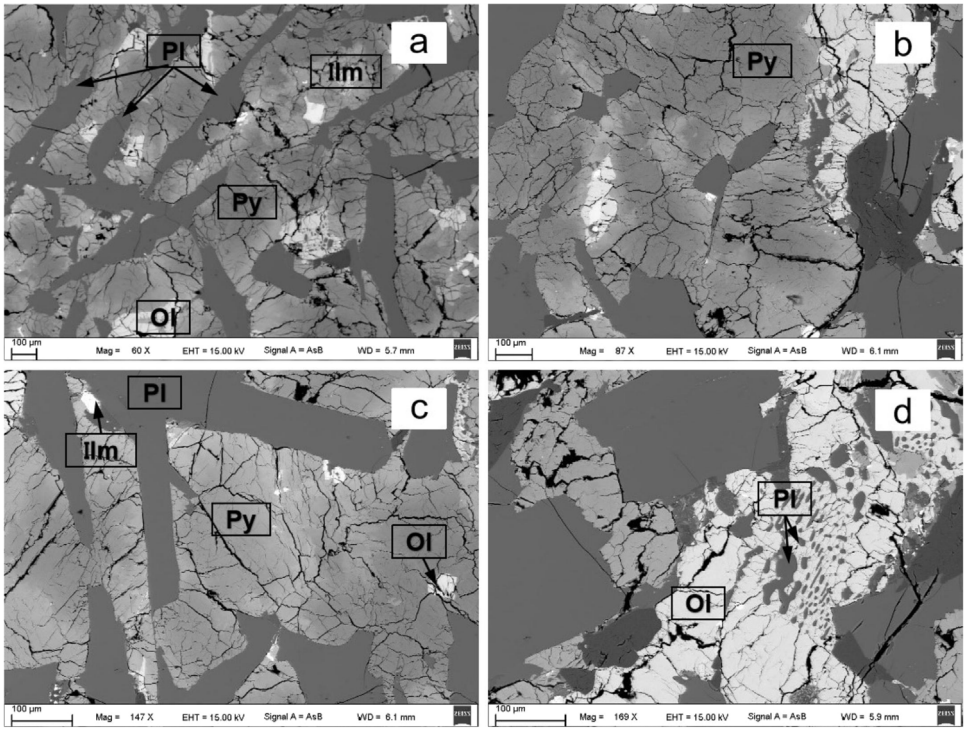

Figure 3. The BSE image of NWA 4734. Pl: plagioclase, Py: pyroxene, Ol: olivine, Ilm: ilmenite. (a) Diabase texture; feldspar oriented distribution; (b) the composition heterogeneity of pyroxene; (c) orthorhombic cleavage of pyroxene: high degree of fragmentation; (d) "Swiss cheese" patten of olivine.

the maskelynite is uniform and has no significant change in composition. However, the pyroxene particles exhibit significant chemical heterogeneity and a high degree of fragmentation (Figure 3(b)). The particles and cracks formed earlier undergo significant displacement after later modification, the crystalline characteristics of which are similar to those of Apollo 12/15 lunar basalts (Chen et al. 2019). Two sets of nearly orthogonal cleavage can be seen on the surface of pyroxene particles (Figure 3(c)), which intersect with coarse cracks and are modified by late-stage cracks. The cleavage of pyroxene particles is developed, and some areas show the appearance of impact melt pocket. Olivine is a semi-idiomorphic phenocryst that in some cases intersects with glassy nodules, forming a "Swiss cheese" pattern (Figure 3(d)), which is a product of highly differentiated residual magma and typical petrographic evidence of magma crystallization differentiation.

By adjusting the brightness, contrast, and setting the greyscale threshold in the BSE image, different minerals could be separated by their greyscale. Then, the minerals' compositions are measured using the EDS and the counted area of each mineral is divided by the total measurement areas to obtain the mineral composition of the NWA 4734 (Figure 4 and Table 1). According to the BSE image and the statistics of minerals' phase distribution diagram (Figure 4), NWA 4734 is mainly composed of pyroxene (61%), plagioclase (28%), olivine (5%), and secondary minerals such as quartz (3%), ilmenite (3%), and spinel (0.2%), as well as a very small amount of troilite. The mineral content results are consistent with previous studies: pyroxene (58.0%) and plagioclase (30.6%), as well as a small amount of olivine (3.8%), ilmenite (2.2%), silica (1.5%), chromite and spinel (0.7%) (Wang et al. 2012b).

Compared with previous studies, the mineral contents in this work show the same characteristics, but there are still some differences. The statistical analysis of mineral contents is based on the surface area counting of minerals, and different cross-sections of samples may also cause some differences in mineral contents.

As shown in Table 2, the numbers of particles identified on the surface of NWA 4734 are 7853; 99.76% of the surface is counted, and the remaining 0.24% is not counted. The reasons are below: (1) minerals are mixed together and cannot be distinguished, which may be remnants of melting or being formed by impact; (2) there are other mineral particles ($<10\ \mu$m) in the mineral, which are smaller than the detection resolution (10 μm) and cannot be counted; (3) crevice.

3.2. Mineralogical Characteristics

EPMA is used to analyze the composition of plagioclase, pyroxene, and olivine in NWA 4734. The plagioclase shows

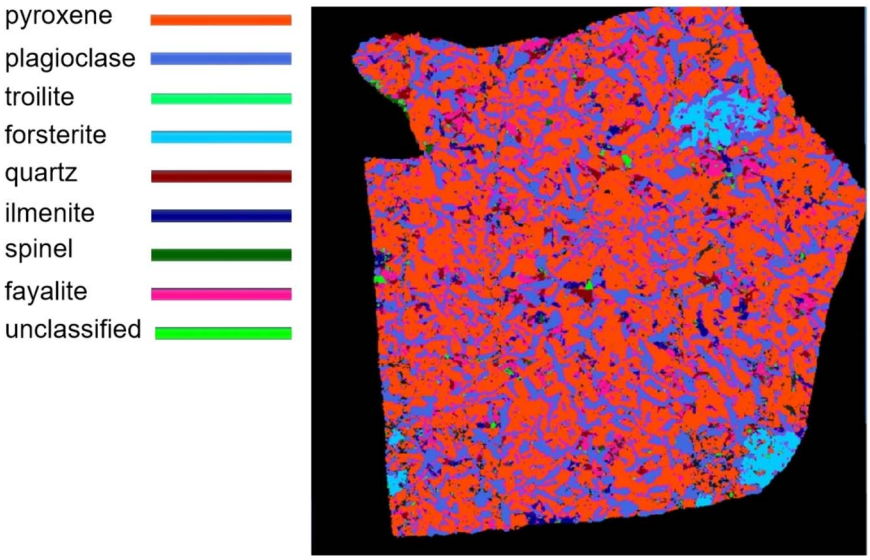

Figure 4. Minerals' composition and distribution on the surface of NWA 4734.

Table 1
Mineral Composition of NWA 4734

Classification	Particles Detected	Total Number of Particles Detected (%)	Area of Classified Particles (μm^2)	Area of Classified Particles (%)
Pyroxene	2024	25.77	1.02×10^8	61.18
plagioclase	2413	30.73	4.7×10^7	28.17
troilite	28	0.36	3.12×10^4	0.04
forsterite	19	0.24	4.54×10^6	2.72
quartz	551	7.02	4.29×10^6	2.57
ilmenite	969	12.34	3.65×10^6	2.18
spinel	246	3.13	5.8×10^5	0.35
fayalite	1129	14.38	3.73×10^6	2.24

high content of CaO (15.8–17.9 wt%), with a relatively uniform composition ($An_{84\text{-}91}Ab_{16\text{-}9}$), which agrees well with previous results (Chen et al. 2019; Wang et al. 2012a). The average An value is 89, which demonstrates that the plagioclase belongs to anorthite and bytownite (Figure 5). The composition of pyroxene varies widely ($Wo_{11–35}En_{3–55}Fs_{26–81}$), which is in the range of augite and pigeonite (Figure 6). The red and blue stars represent the composition of the pyroxenes' core and rim respectively, which clearly show that the pyroxene composition is heterogeneous with a higher magnesium content in the core and a higher iron content in the rim. The previous research results were $Fs_{23–87}Wo_{12–42}En_{1–59}$, which is consistent with our results. The slight difference comes from the randomness of the measurement points (Chen et al. 2019). The composition heterogeneity of olivine is also large, with a variation range of Fa index (molar Fe/(Mg+Fe)) of 57–90 (Figure 6). Wang reported that Fa index varied from 33 to 92 in previous research (Wang et al. 2012a). The reason for the difference is that the range of olivine composition is very large, and the low content of olivine is not conducive to selecting enough points to measure. Similarly, the red and blue stars are used to distinguish the composition of the core and rim, respectively. It can also be seen that the composition of olivine is heterogeneous with a higher magnesium content in the core and a higher iron content in the rim, providing clear evidence of magmatic differentiation.

3.3. The Proportion of HCP Calculated from Image Pixel Counting

The area marked with a red circle in the BSE image (Figure 2) shows the region where the proportion of HCP is statistically counted in terms of pixels. The visible and near-infrared spectra of this region measured by ASD will also be modeled by MGM, to retrieve the proportion of HCP in total pyroxenes. The statistical image pixel counting results will be used as a standard to assess the applicability and accuracy of MGM. Therefore, it is crucial to accurately determine the proportion of HCP in this region using the image pixel counting method. Like the method described in Section 2.4, the proportion of HCP in 21 BSE images (Figure 7) of the circular area was calculated using the pixel counting method, and the statistics are shown in Table 3. As displayed in Figure 7, the pixels with red colors represent the HCP while the pixels with blue colors represent the LCP. The total number of LCP pixels is 1,913,565, and the total number of HCP pixels is 3,635,247. We could obtain the proportion of HCP by the ratio of the total number of HCP pixels to the total number of HCP and LCP, and the calculation result is 65.5% according to the statistics.

Table 2
The Numbers of Particles Identified on the Surface of NWA 4734

Classification	Particles Detected	Total Number of Particles Detected (%)	Area of Classified Particles (μm^2)	Area of Classified Particles (%)
All Particles Detected	7853	100	1.67×10^8	100
Classified	7617	96.99	1.67×10^8	99.76
Unclassified	236	3.01	3.99×10^5	0.24

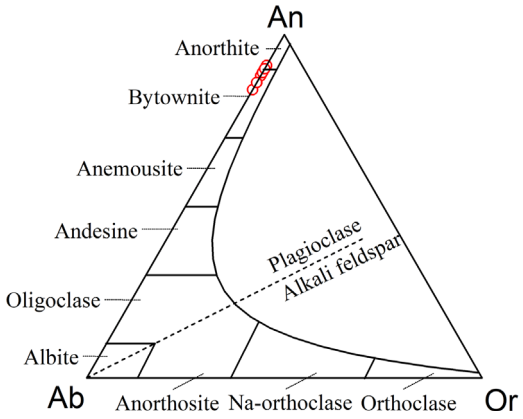

Figure 5. Feldspar composition of NWA 4734.

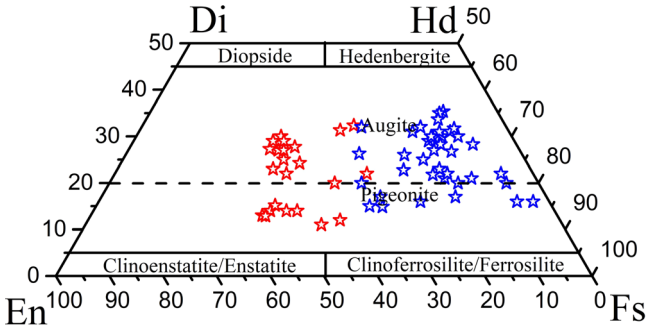

Figure 6. Classification diagram of pyroxene and olivine in NWA 4734.

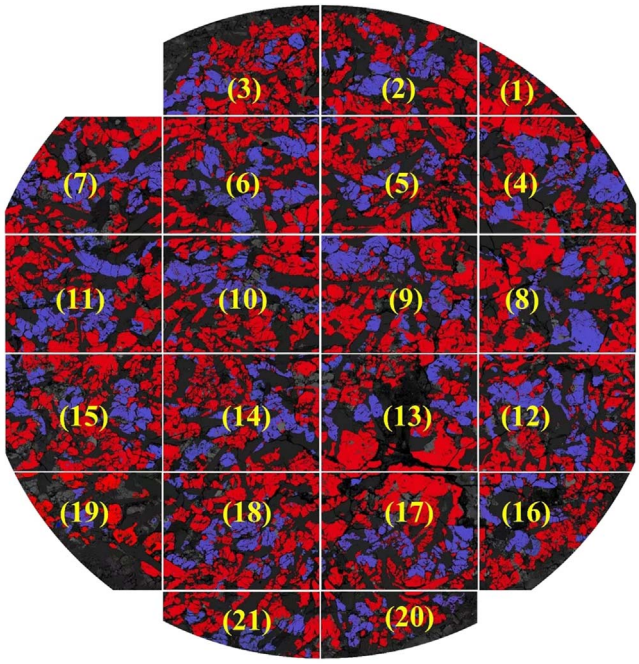

Figure 7. Calculating the proportion of HCP using the image pixel counting method. The BSE image of the red circle in Figure 2 is divided into 21 parts. The pixels with the red colors represent HCP, and the pixels with the blue colors represents LCP.

Because the modal abundance of the image pixel counting is two-dimensional (areal) data while the spectral data reflect the three-dimensional (volumetric) modal abundance, the former data should to be converted to be comparable with the latter data. Customarily, this is done by applying the power of 3/2 (Pieters 1993). When converted in that way, the HCP ratio becomes 0.723 (72%) based on the image pixel counting modal.

3.4. The Proportion of HCP Calculated from MGM Deconvolution

The visible and near-infrared spectra of the same red circular area in Figure 2 is obtained by ASD. As demonstrated in Figure 8, NWA 4734 exhibits significant absorption features at ~1000 and ~2200 nm, with a significant asymmetry in the absorption feature at ~1000 nm, and a significant plagioclase or olivine absorption feature near 1250 nm. The spectra of NWA 4734 show the typical absorption features of lunar mare basalts.

MGM was applied to deconvolve the spectra of NWA 4734 to constrain the proportion of HCP. The software developed by the Reflectance Experiment Laboratory (Relab; http://www.planetary.brown.edu/relab/) was used. The identified spectral features imply the presence of pyroxene and olivine, so eight Gaussian bands are used to deconvolve the spectra; the results are depicted in Figure 9, and the spectral fitting error (RMSE) is <1.4%. The fitted parameters of pyroxenes are listed in Tables 4 and 5.

The proportion of HCP can be quantified by calculating the "component band strength ratio (CBSR)" (Sunshine & Pieters 1993). As affirmed in Figure 10, the CBSR varies logarithmically with the proportion of HCP. The comparison

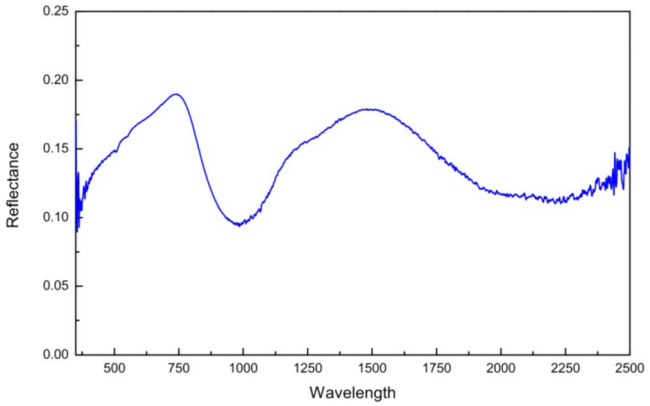

Figure 8. NWA 4734 spectral curve measured by the ASD.

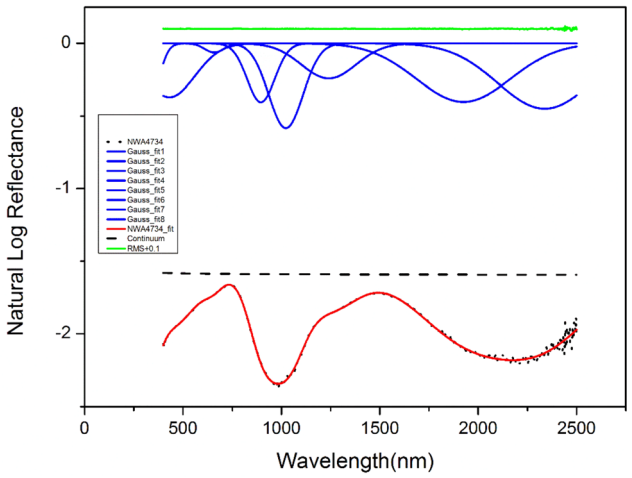

Figure 9. Spectral fitting results of NWA 4734 using MGM.

Table 3
The Pixel Counting Results of HCP and LCP

	Number of Pixels of LCP (Blue Area)	Number of Pixels of HCP (Red Area)
01	48,558	104,098
02	83,493	172,548
03	84,256	159,205
04	127,506	208,671
05	90,357	217,135
06	134,328	213,977
07	125,620	219,693
08	116,443	227,100
09	125,610	201,706
10	101,501	204,377
11	131,190	190,166
12	125,953	174,111
13	85,075	199,640
14	98,894	188,553
15	95,146	212,696
16	58,582	111,408
17	96,385	207,615
18	95,249	195,205
19	16,610	65,805
20	40,401	67,663
21	32,408	93,875
Total	1,913,565	3,635,247
Percent of HCP	65.5%	

Table 4
Spectral Parameters at ∼1 μm after MGM Fitting

Fitted Gaussian Curves	Spectral Parameters of MGM Fitting	
Gauss-fit4	center wavelength	896.0 nm
	full width at half maximum	165.4 nm
	band strength	−0.404
Gauss-fit5	center wavelength	1022.9 nm
	full width at half maximum	190.2 nm
	band strength	−0.465

Table 5
Spectral Parameters at ∼2 μm After MGM Fitting

Fitted Gaussian Curves	Spectral Parameters of MGM Fitting	
Gauss-fit7	center wavelength	1925.2;nm
	full width at half maximum	564.0 nm
	band strength	−0.402
Gauss-fit8	center wavelength	2338.5 nm
	full width at half maximum	563.6 nm
	band strength	−0.449

between Figure 10(a) and (b) shows that the relationship between the CBSR and the proportion of HCP at 1 and 2 μm is almost the same. After MGM fitting, the CBSR of the NWA 4734 at 1 and 2 μm can be obtained. By calculating the CBSR at 1 μm between the Gaussian curves fit-4 and fit-5 ($-0.404/-0.465 = 0.869$), the proportion of HCP can be estimated as 67%–75% according to the logarithmical relationship. Similarly, by calculating the CBSR at 2 μm between MGM fitted Gaussian curves fit-7 and fit-8 ($-0.402/-0.449 = 0.895$), the proportion of HCP can also be estimated as 66%–73%. So, the average proportion of HCP is 71%. This model error is about 5%–10% (Sunshine & Pieters 1993).

3.5. Error Analysis and Applicability of MGM

We have obtained the proportion of HCP in meteorite NWA 4734 using two methods: the image pixel counting and the MGM model, and it is necessary to conduct a thorough discussion of errors and their sources.

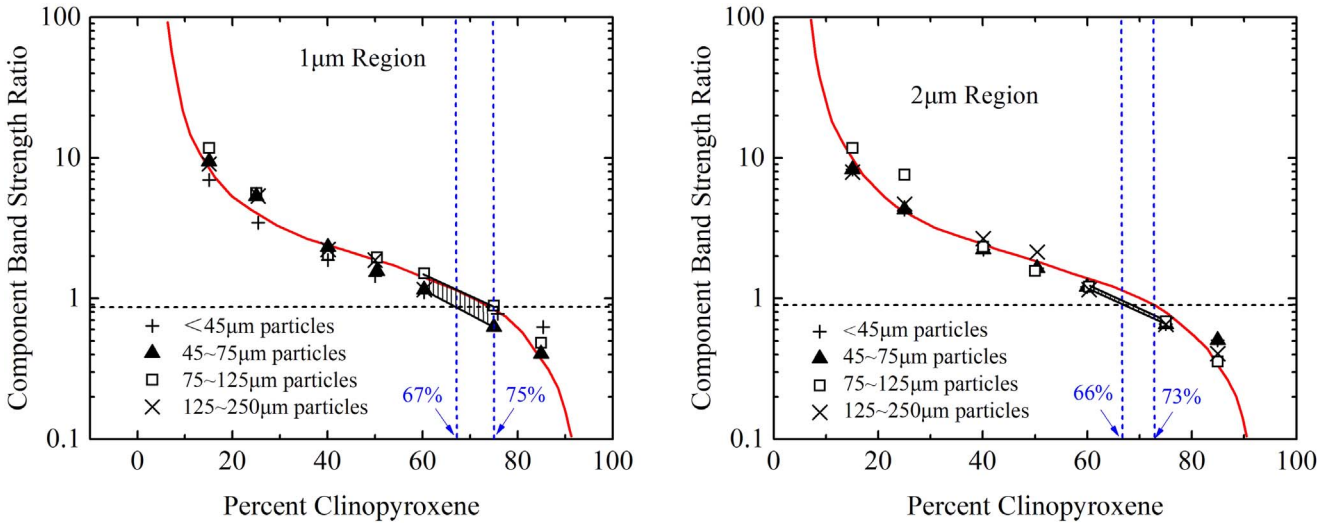

Figure 10. The logarithmical relationship between the CBSR and the proportion of HCP. (a) the relationship at the 1 μm region, (b) the relationship at the 2 μm region (Sunshine & Pieters 1993).

The main sources for the errors included two factors: the methods we used and the instrument measurement. A tolerance of 5% is set in the pixel counting method, which may cause errors in gray scale recognition. Besides, there is ∼2% of uncounted area by cracks and unrecognized minerals. So, the RMSE of the pixel counting method is ∼5.4%, and the proportion of HCP calculated from the pixel counting method should be $72\% \pm 5.4\%$.

The errors for the MGM method are mainly contained in two factors: the spectral fitting error (<1.4%) and the modal error between the CBSR and the proportion of HCP (<10%) (Sunshine & Pieters 1993). So, the RMSE for MGM modeling is <10.1% and the proportion of HCP calculated from the MGM method should be $71\% \pm 10.1\%$.

Moreover, the errors caused by the instrument measurement are mainly caused by the difference in the surface area measured by the ASD and the SEM. The red circle shown in Figure 2 is marked after the spectral measurement of ASD, and we try our best to simultaneously obtain the minerals' content at the same location by SEM and EDS. However there are still measurement errors, and it is difficult to quantify error, so we give an estimate of error to be ∼3%.

After the error analysis, we think that the proportion of HCP derived from MGM is comparable to the result derived from the pixel counting method, and the MGM can be applied to in situ spectral analysis and mineral quantification of lunar rock samples.

4. Conclusion

The estimation of the ratio between HCP and LCP contents is of great significance for constraining the origin and evolution of the lunar rock targets. The MGM has important applications in identifying the minerals' composition and the modal abundance of pyroxene end-members (HCP and LCP). It is generally believed that the quantification accuracy of pyroxene end-members' modal abundances are within 10% when the olivine content does not exceed 15%. However, this method is mainly applied to interpretation of laboratory and remote sensing powder samples, and its applicability and accuracy on rock sample quantification remain to be further evaluated. This study focuses on the lunar meteorite NWA 4734 as a representative sample to provide important ground truth for the interpretation of lunar surface rock samples. NWA 4734 has been extensively studied in petrology, mineralogy, and chronology, but there is little work on in situ spectral measurement and analysis. We first analyze the petrological and mineralogical characteristics of NWA 4734, confirming that NWA 4734 has undergone severe shock melting metamorphism, with plagioclase almost completely converted into maskelynite. Pyroxene and olivine exhibit significant chemical composition heterogeneity, with a core rich in magnesium and a rim rich in iron, further indicating that NWA 4734 has undergone multiple crystallization and differentiation processes. Second, two different methods are performed to estimate the proportion of HCP on the rock surface of NWA 4734: (1) the BSE image of NWA 4734 is greyscale processed to distinguish HCP and LCP, and then the image pixel counting method is used to calculate the proportion of HCP in the total pyroxene as $72\% \pm 5.4\%$; (2) the visible and near-infrared spectra of the rock NWA 4734 are obtained by an ASD spectrometer, and the MGM deconvolution method is used to calculate the CBSR and to quantify the proportion of HCP in the total pyroxene as $71\% \pm 10.1\%$. The results derived from the two methods are comparable, which demonstrates that

the MGM can be applied to in situ spectral analysis and mineral quantification of lunar rock samples.

ORCID iDs

Bin Liu https://orcid.org/0000-0002-4875-3429

References

Cheek, L. C., & Pieters, C. M. 2014, AmMin, 99, 1871
Chen, J., Jolliff, B., Wang, A., et al. 2019, JGRE, 124, 2583
Clénet, H., Pinet, P., Daydou, Y., et al. 2011, Icar, 213, 404
Crown, D. A., & Pieters, C. M. 1987, Icar, 72, 492
Elardo, S. M., Shearer, C. K., Jr., Fagan, A. L., et al. 2014, M&PS, 49, 261
Fernandes, V., Korotev, R., & Renne, P. 2009, in 40th Lunar and Planetary Science Conf. (Lunar and Planetary Science XL), 1045
Gendrin, A., Bibring, J.-P., Mustard, J., et al. 2006, LPSC XXXVII, Houston (USA), Abstract, 1858
Isaacson, P. J., & Pieters, C. M. 2010, Icar, 210, 8
Jambon, A., & Devidal, J.-L. 2009, M&PSA, 72, 5006
Kanner, L. C., Mustard, J. F., & Gendrin, A. 2007, Icar, 187, 442
Mustard, J. F., Murchie, S., Erard, S., & Sunshine, J. 1997, JGRE, 102, 25605
Mustard, J. F., & Sunshine, J. M. 1995, Sci, 267, 1623
Noble, S. K., Pieters, C. M., Hiroi, T., & Taylor, L. A. 2006, JGRE, 111, E11009
Pieters, C. 1993, Remote Geochemical Analysis Elemental and Mineralogical Composition, Vol. 309 (Cambridge: Cambridge Univ. Press), 9
Pieters, C. M., Head, J., Sunshine, J., et al. 1993, JGRE, 98, 17127
Sunshine, J. M., & Pieters, C. M. 1993, JGRE, 98, 9075
Sunshine, J. M., & Pieters, C. M. 1998, JGRE, 103, 13675
Sunshine, J. M., Pieters, C. M., & Pratt, S. F. 1990, JGRB, 95, 6955
Wang, Y., Guan, Y., Hsu, W., & Eiler, J. 2012a, M&PSA, 75, 5170
Wang, Y., Hsu, W., Guan, Y., et al. 2012b, GeCoA, 92, 329